BOUNDARY CONDITIONS FOR LATERAL DEFORMATION OF WEBS TRANSITING ROLLERS IN ROLL-TO-ROLL PROCESS MACHINES

By

J. K. Good, Yao Ren and Jinxin Shi
Oklahoma State University
USA

ABSTRACT

The lateral deformations of webs in roll-to-roll (R2R) process machines can affect the quality of the manufacturing process. The lateral registration of the web in successive R2R processes can determine whether a product will function as designed. Herein a unified theory is presented that explains how imperfections in rollers, their alignment and length nonuniformity (camber) in webs can affect the steady state lateral deformation and hence registration. Enhanced understanding of steady state lateral deformation of webs transiting free spans and rollers will provide insight for advanced control methods that account for the effects of web deformation in minimizing registration error. The validated results show that the lateral deformations can be predicted with closed form equations. In some cases the boundary conditions which are integrated into these equations must be determined using dynamic simulation.

INTRODUCTION

The ability to predict and control the lateral deformation of webs transiting through roll-to-roll process machines is important. Often webs undergo multiple processes where discrete coatings must be deposited precisely with respect to previous coatings. Gravure coating is used for fine multicolor printing and printed electronics. In these processes successive print rollers are overlaying coatings precisely with respect to coatings deposited by previous rollers. When the successive coatings are not deposited in the lateral location intended a registration error has occurred. This error could produce a blurred image unpleasing to the eye or a malfunction in the case of printed electronics.

The objective of this publication is to provide a unified theory regarding the boundary conditions between webs and rollers which dictate the lateral deformations of the web for simple and then more complex cases. Webs are often treated as beams between rollers. Shelton was first to discover how a web is laterally steered by a misaligned roller [1,2]. Shelton's discovery was triggered by experimental observation. In these tests he misaligned a downstream roller in a test span and measured the lateral

deformation that resulted after steady state conditions were achieved. Shelton limited the misalignment to ensure that moments generated at the upstream roller did not surpass the moment that could be reacted by friction between the web and roller [3,4]. This confined the lateral deformations to his test span and resulted in a constant lateral deformation in downstream spans. From his test results, Shelton inferred the lateral deformations for long spans were governed by boundary conditions including (1) the lateral deformation of the web entering the test span was zero, (2) the slope of the web entering the span was zero for long spans where shear deflections were small, (3) that the slope of the web entering the misaligned roller was the misalignment of the roller (the normal entry condition) and (4) that the moment was zero in the web at entry to the misaligned roller. Yurtcu et. al. [5] successfully performed a similar analysis and tests for a web span with a downstream roller whose radius tapered linearly across the roller width and derived the four boundary conditions needed to quantify the lateral deformations of the web in the test span. These investigations both treated the web span between two rollers as a beam whose lateral deformations were dictated by kinematic and kinetic boundary conditions imposed at the ends of the beam. Both investigations treated the effects of web tension on lateral deformation.

A more complex case is that of the cambered web. A cambered web is a web with one side longer than the other. If a length of such a web is smoothed upon a flat surface, the web takes on the appearance of a curved beam. The camber can be quantified by measuring the radius of curvature of the elastic axis of the unstressed web (ρ_o). Experimental investigations on cambered webs in belt form [6] and on cambered webs transiting through roll-to-roll process machines [7,8] have consistently shown that the web steers towards the longer edge. Modelling efforts have been less successful in comparison to the experiments [8-16] and will be discussed later.

This publication will deviate from these previous analyses by considering how the mechanics of the web transiting a roller can dictate the lateral behavior of the web in a free span. These considerations will be given to the previous cases of a web span with a downstream misaligned or tapered roller and then to the more complex case of a cambered web.

DISCUSSION

The lateral deformation *v* of a beam of bending stiffness *EI* subjected to tension *T*, lateral loads, bending moments but the absence of lateral tractions are governed by the differential Equation {17}:

$$EI\frac{d^4v}{dx^4} - T\frac{d^2v}{dx^2} = 0 \qquad \{1\}$$

The solution of the differential equation is of the form:

$$v = A + B\frac{x}{L} + C * \cosh\left[\frac{\lambda x}{L}\right] + D * \sinh\left[\frac{\lambda x}{L}\right] \quad \lambda = \sqrt{\frac{TL^2}{EI}} \qquad \{2\}$$

where *x* is coordinate taken on the elastic axis of a beam of length *L*. The constant coefficients *A*, *B*, *C* and *D* depend on the boundary conditions for the problem under attack. Examples of straight webs entering misaligned rollers and tapered rollers will be examined for which closed form solutions of the differential equation can be developed. The solution of a cambered web transiting aligned rollers will be addressed.

A Web Approaching a Misaligned Roller

A web exits an upstream roller in a web span. It will be assumed that the web entered that roller under the condition of normal entry posed by Lorig [18]. The condition of normal entry is one in which the elastic axis of the web is orthogonal to the axis of rotation of the upstream roller. The web will have zero lateral velocity on the upstream roller and the lateral position of the elastic axis of the web will be arbitrarily set at zero. Furthermore it will be assumed that the available friction forces between the web and the upstream roller are sufficient to prevent any slippage of the web laterally or in rotation on the roller surface. With these assumptions the lateral deformation and slope of the web exiting the upstream roller can be assumed to be zero:

$$v_i = v(0) = 0 \qquad \{3A\}$$

$$\theta_i = \left.\frac{dv}{dx}\right|_{x=0} = 0 \qquad \{3B\}$$

The downstream roller is misaligned at an angle θ orthogonal to the plane of the web span. If the misalignment occurred instantaneously the web would begin to translate laterally on the downstream roller. Webs respond to dynamic disturbances much as a first order dynamic system would react to a step input. Webs typically have very little mass which minimize internal inertial loads and allows the approximation of a first order system. After about 4 time constants τ, where $\tau = L/V$, L is the span length and V is the web velocity, the web would come to a new steady state lateral location on the misaligned roller and dynamic motion would cease. The web has now achieved normal entry to the misaligned roller. The slope of the web at the entry to the misaligned roller θ_j will have become equal to the misalignment θ:

$$\theta_j = \left.\frac{dv}{dx}\right|_{x=L} = 0 \qquad \{3C\}$$

Furthermore due to the assumption of no slippage of the web on the misaligned roller, the slope of the elastic axis of the web will remain at θ as the elastic axis follows a curvilinear path around the misaligned roller. Since the slope is not changing, the derivative of the slope must be zero:

$$\left.\frac{d^2v}{dx^2}\right|_{x=L} = \left.\frac{d\theta}{dx}\right|_{x=L} = 0 \qquad \{3D\}$$

The four boundary conditions presented in Equations {3A-3D} are sufficient to determine the four unknown coefficients A-D in Equation {2}. The equation for the lateral deformation of the elastic axis of web in the free span between the upstream roller and the downstream misaligned roller is:

$$v = \frac{\lambda x \cosh(\lambda) + L\left(\sinh\left(\lambda(1 - x/L)\right) - \sinh(\lambda)\right)}{\lambda(\cosh(\lambda) - 1)}\theta \qquad \{4\}$$

This equation has been validated by tests [19]. A polyester web 15.24 cm wide and 23.4 μm in thickness was transported through a web span 45.72 cm in length. Young's modulus of the web was tested and found to be 4.90 GPa. Web tension was set at 13.3 N. In Figure 1 the lateral deformations predicted by {4} and the test results are presented. Note the agreement between tests and {4} is quite good at low misalignment but that the

result from {4} becomes less than the test data at greater misalignments. The length to width ratio of the web span is 3 and as such it might be argued that shear deformations could be significant. Also the friction forces between the web and the upstream roller surface may have been insufficient to restrain the bending moment that is maximum at that location and increases proportionately with misalignment. Thus the slope of the web exiting the upstream roller may have been greater than zero due to slippage. Either one of these sources of error could be sufficient to explain the difference seen between the lateral deformations predicted by {4} and the test results. Also note that shearing deformation and slippage would both result in test results that would be greater than the prediction by Equation {4} since neither effect was taken into account in the derivation. Nevertheless the agreement shown in Figure 1 is sufficient to prove that the downstream curvature boundary condition {3D} is valid.

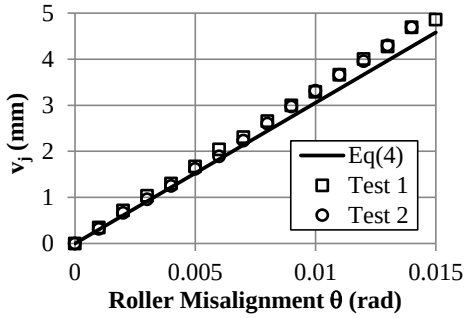

Figure 1 – Lateral Deformations of a Web due to a Downstream Misaligned Roller

Shelton [2] was first to demonstrate the analysis of a web approaching a misaligned roller. He implemented boundary conditions {3A-3C} above. His 4th boundary condition was determined experimentally in the laboratory. He determined that the moment in the web at the entry to the downstream roller was zero.

$$M_L = 0 \qquad \{5\}$$

Shelton also determined that a lateral force at the downstream roller was required to achieve normal entry {3C}:

$$N_L = \frac{T\theta}{\cosh(\lambda)-1} \qquad \{6\}$$

He derived an equation equivalent to {4} for the lateral deformation. While the difference may seem inconsequential the argument presented is that Shelton's kinetic boundary conditions {6} and {5} were needed to sustain the kinematic boundary conditions {3D} and {3C}, both of which rely on no slippage in the entry region of the web on the misaligned downstream roller.

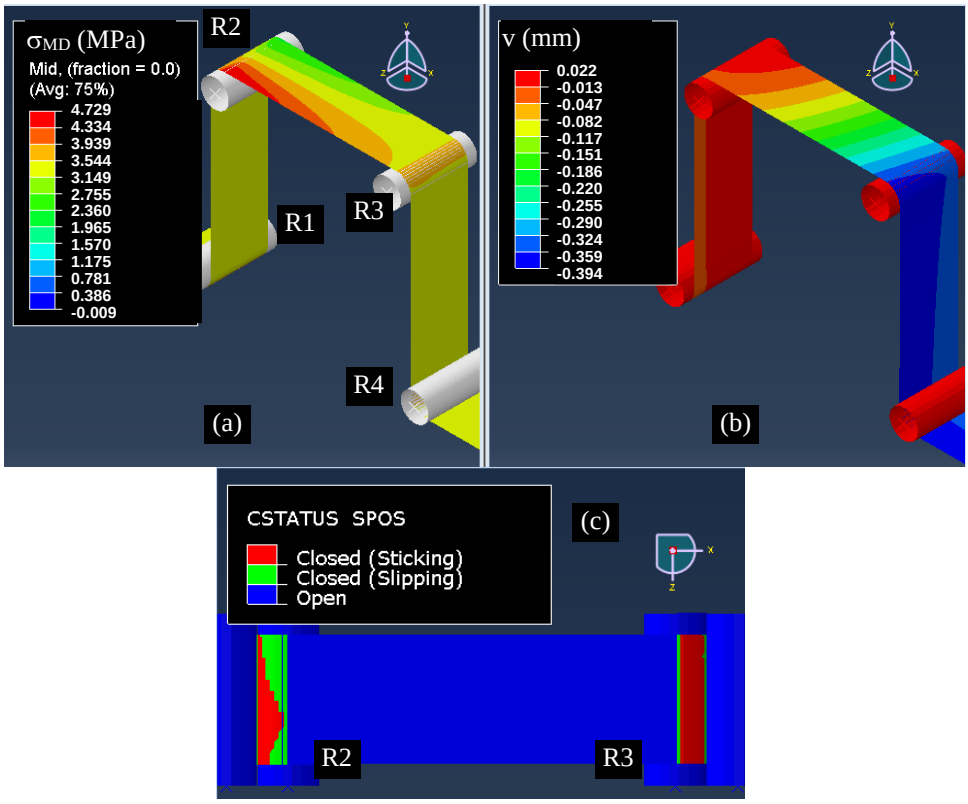

Figure 2 – Dynamic Simulation of a Web Approaching a Misaligned Roller

A dynamic finite element simulation[1] code was used to provide means of visualizing the behavior discussed. The horizontal span of web in Figure 2a has identical length, width, thickness and modulus to the web described earlier in the tests. The 3rd roller in the simulation (R3) was given a misalignment of 1 mrad about the y axis in Figure 2a. A web length 4 times the span length between rollers R2 and R3 was allowed to pass over the rollers in the simulation. Web tension was maintained 12.3 N, slightly less than the tests conducted at 13.3 N. In Figure 2a the web travels in the x direction. Note the MD stresses become uniform as the web enters roller R3. This uniformity in stress demonstrates the moment about the y axis on the elastic axis of the web is zero, hence Shelton's condition {5} is satisfied. The lateral deformations are shown in Figure 2b. In the vertical entry span the lateral deformations are due to uniform Poisson contraction. In the horizontal test span the lateral deformations are due to a combination of Poisson contraction and lateral steering. Finally in the vertical exit span the deformations are to the steering in the horizontal span, Poisson contraction and the slight twist the span is subject to. The presence of stick and slip behavior between the web and the entry (R2) and exit (R3) rollers is shown in Figure 2c. Note that stick behavior occurs over most of the contact

[1] Dassault Systems, Abaqus Simulia, Rising Sun Mills, 166 Valley St., Providence, RI 02909-2499

between the web and roller R3. The MD stress variation shown across the width of the web as the web exits roller R2 results in varying degrees of capstan slippage across R2 as shown in Figure 2c. The level of slippage will jeopardize the validity of boundary condition {3B}.

The lateral deformations for the elastic axis of the web were harvested from the whole field data presented in Figure 2b and presented in Figure 3. The lateral deflection of the elastic axis at the entry to R3 is -.327 mm (-.013 in). In Figure1 the average absolute test deflection from the two tests is 0.331 mm, thus the simulated value is within 1.2% of the test value. Both the simulations and the tests allow slippage at the exit of R2 and relaxation of condition {3B}. Equation {4} produces a deflection of -.305 mm, 7.8% in error compared to the test value. For this condition, Equation {6} predicts a lateral force of 0.271 N is required to enforce normal entry of the web to roller R3. The results of the dynamic simulation showed that a lateral load of 0.260 N was required, very comparable to that predicted from Equation {6}.

The dynamic simulation has none of the boundary conditions {3A-3D} enforced but the displacements, slopes and curvatures presented in Figure3 show these boundary conditions are reasonable. In Figure 3 the web exits the upstream roller R2 at an MD location of 0 cm. The web enters roller R3 at 45.72 cm. The MD Location is a coordinate that follows the elastic axis of the web as it wraps around roller R2, proceeds into the horizontal span and then wraps roller R3. The web exits R2 with no lateral deformation {3A} and little slope {3B}. The web enters R3 at the slope of the misaligned roller {3C} with near zero curvature {3D}.

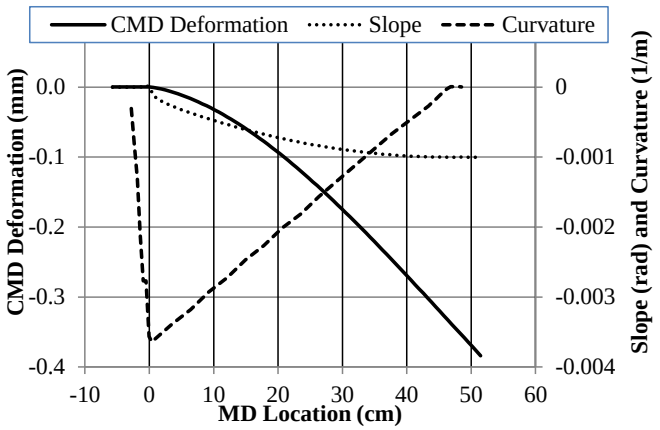

Figure 3 – Deformation, slope and curvature of the elastic axis of the web after steady state conditions were achieved in the simulation shown in Figure 2.

In Figure 4 the rate that the steady state boundary conditions were achieved in the simulation are shown. The dynamic time constant is the span length (45.7 cm) divided by the web velocity (7.37 cm/s) or 6.2 seconds. It appears that steady state conditions had been attained after 20 seconds of simulation or about 3.2 time constants.

The web wrapping the misaligned roller is a sector of a right circular cylinder whose inside surface matches the outside surface of the misaligned roller precisely as shown in Figure 5(a). That these shapes match precisely allows the web to cross much of the misaligned roller R3 without slip. The lateral force N_L was required to achieve normal

entry. The zero curvature allows the elastic axis to follow a circular rather than a helical path in the entry region of R3.

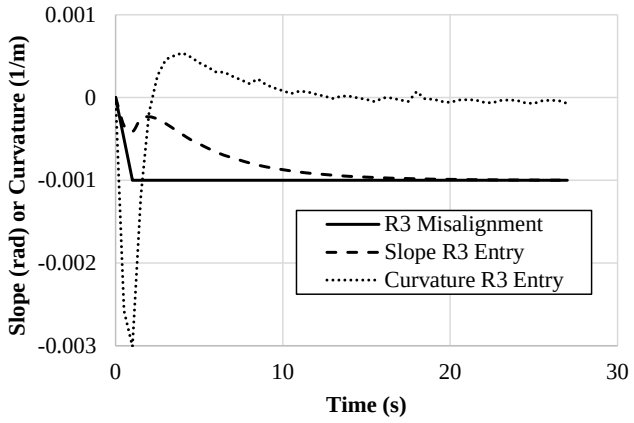

Figure 4 – Rate at which steady state boundary conditions are attained in the simulation shown in Figure 2.

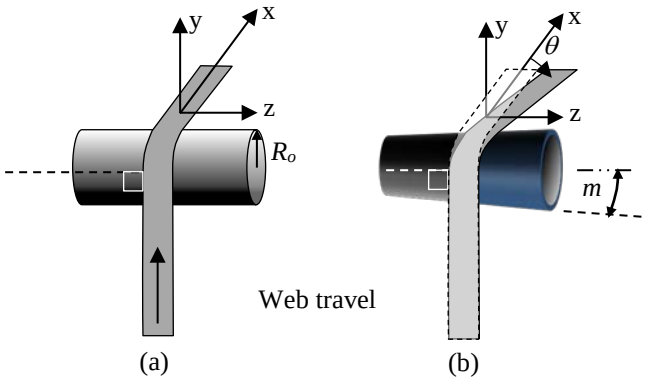

Figure 5 – A Web Entering (a) a Cylindrical Roller and (b) a Tapered Roller Normally

A Web Approaching a Tapered Roller

Rollers can take the shape of a truncated cone as an unintentional result of manufacturing processes. Manufacturers of rollers will quote the maximum radial taper m as an error in the radius of the roller per unit width (in the CMD). A tapered roller will steer a web in the CMD towards the larger radius end of the roller. Assume an upstream roller is a perfect right circular cylinder. Also assume the next roller downstream is a roller with linear radial taper m with respect to the CMD. The nominal radius of this roller R_o is defined halfway across the roller width. Furthermore, assume the axes of rotation of both rollers are parallel and hence they are aligned. In Figure 5 a straight web is shown entering a cylindrical roller (a) and a tapered roller (b) under normal entry conditions. Assume temporarily that the web is under no stress but that it is forced to have surface contact with the rollers and consider the geometry. The web exiting the

cylindrical roller will exit normally to the exit tangent line. The web exiting the tapered roller will not exit normally but at an angle θ given by:

$$\theta = \phi m = \frac{s}{R} m \qquad \{7\}$$

where ϕ is the wrap angle of the web about the roller and s is a curvilinear coordinate following the elastic axis of the web. The earlier assumption of allowing no slippage will not allow the web to follow this path. If the web does not slip it will proceed straight over the roller as shown in the dashed configuration in Figure 5(b) which makes it appear similar to the web in Figure 5(a). Now the web must be deformed in a negative θ direction to allow the web to travel directly over the roller and exit normally from the tapered roller. To accomplish this, a constant curvature must be enacted on the web so that the straight dashed path can be followed without slip:

$$\left.\frac{d^2v}{ds^2}\right|_{x=L} = -\left.\frac{d\theta}{ds}\right|_{x=L} = -\frac{m}{R_o} \qquad \{8\}$$

The four boundary conditions {3A} and {3B}, {3C} with θ = 0 and {8} were used in conjunction with Equation {2} to determine the unknown coefficients A, B, C and D. The equation for the lateral deformation of an initially straight web approaching a tapered roller is:

$$v = \frac{mEI}{R_o T}\left[\cosh\left[\frac{\lambda x}{L}\right] - 1 + \coth\left[\frac{\lambda}{2}\right]\left(\frac{\lambda x}{L} - \sinh\left[\frac{\lambda x}{L}\right]\right)\right] \qquad \{9\}$$

From Equation {9}, the moment and shear in the web at the entry to the tapered roller can be determined:

$$M_L = EI\left.\frac{d^2v}{dx^2}\right|_{x=L} = \frac{mEI}{R_o} \qquad \{10\}$$

$$N_L = EI\left.\frac{d^3v}{dx^3}\right|_{x=L} = \frac{m\sqrt{TEI}}{R_o}\coth\left[\frac{\lambda}{2}\right] \qquad \{11\}$$

This is the lateral load {11} required to enact normal entry {3C} and thus steady state lateral deformation. The moment {10} is required to enact the constant curvature {8} that will allow the elastic axis of the web to travel directly over the roller with no slip, shown in the dashed path in Figure 5(b). Yurtcu et al [5] developed similar equations for {10} and {11} assuming a polynomial deformation function in {9} which accounted for the effects of tension and shear stiffness.

Equation {9} has been validated in tests as shown in Figure 6. A polyester web 15.24 cm wide and 23.4 μm in thickness was transported through a web span 50.8 cm in length. Young's modulus of the web was tested and found to be 4.90 GPa. Web tension was set at 44.5 N. Four tapered rollers with tapers m of 0.00028, 0.00054, 0.00064 and 0.00075 radians with a nominal radius R_o of 3.76 cm were machined for these tests. Reasonable agreement between the tests and Equation {9} is demonstrated. Note the test results are slightly larger than those predicted by Equation {9}, a behavior similar to that witnessed for the web encountering a downstream misaligned roller in Figure 1.

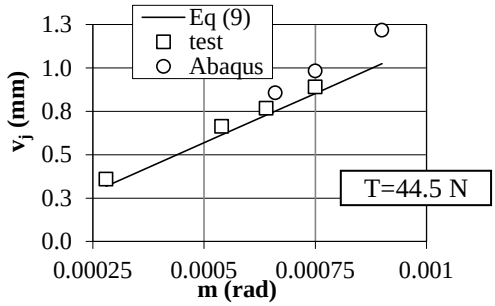

Figure 6 – Lateral Deformations of a Web due to a Downstream Tapered Roller

Dynamic simulations of a web transporting through a span with a downstream tapered roller were conducted[1]. The web width, thickness and span length and the material properties were identical to the test conditions. Results for the lateral deformation of the elastic axis at the entry to the tapered roller are shown for roller tapers *m* of 0.00066, 0.00075 and 0.0009 m/m in Figure 6. Simulation results are shown in Figure 7 for the roller taper of m=0.00066 m/m.

In Figure 7(a), rollers R1, R2 and R4 are cylindrical with an outer radius of 3.68 cm. Roller R3 is the tapered roller whose nominal radius at the center is 3.68 cm and whose taper *m* in this case is 0.00066 rad. The web tension was set to 44.5 N. The web travels from left to right in these simulations. For the simulation to achieve steady state MD stresses and lateral deformations, shown in Figs. 7(a) and (b), the web had to move over 200 cm in the MD. Note how the MD stresses remain constant as the web transports over the tapered roller R3. This is an indication that the curvature of the elastic axis of the web on the roller is constant. Also note the deformation contour in Figure 7(b) moves directly over the roller which indicates the lateral deformation at a given CMD location is constant. This is seen in greater clarity in Figure 8 which shows the lateral deformation, slope and curvature of the elastic axis of the web in steady state conditions harvested from the simulation results shown in Figure 7. The web exits roller R2 at MD location 0 and enters R3 at 50.8 cm. The results shown in Figure 8 demonstrate clearly that the lateral deformation of the elastic axis of the web is constant as the web moves over roller R3 and is indicative of stick behavior between the web and roller surface. As the web exits R3 slippage will occur and the lateral deformations will vary in the slip region. Note the elastic axis enters R3 normally and remains normal through the entry stick region. The curvature is linear through the free span before becoming constant on roller R3. As the web enters R3 the simulation results show the web curvature is -0.01783 m^{-1}. This compares well with the curvature boundary condition for stick conditions {8}: -m/Ro = -0.00066/0.0368=-0.01794 m^{-1}, only 0.62% different. Thus the curvature boundary condition {8} is valid. Also the simulation shows the slope to be zero at R3 entry (hence normal entry) and boundary condition {3C} appears reasonable. Note the slope at the exit of R2 is small but non-zero (0.0037 rad), which contributed to the simulated deformation at the entry to R3 being greater than the test and Equation {9} values in Figure 6.

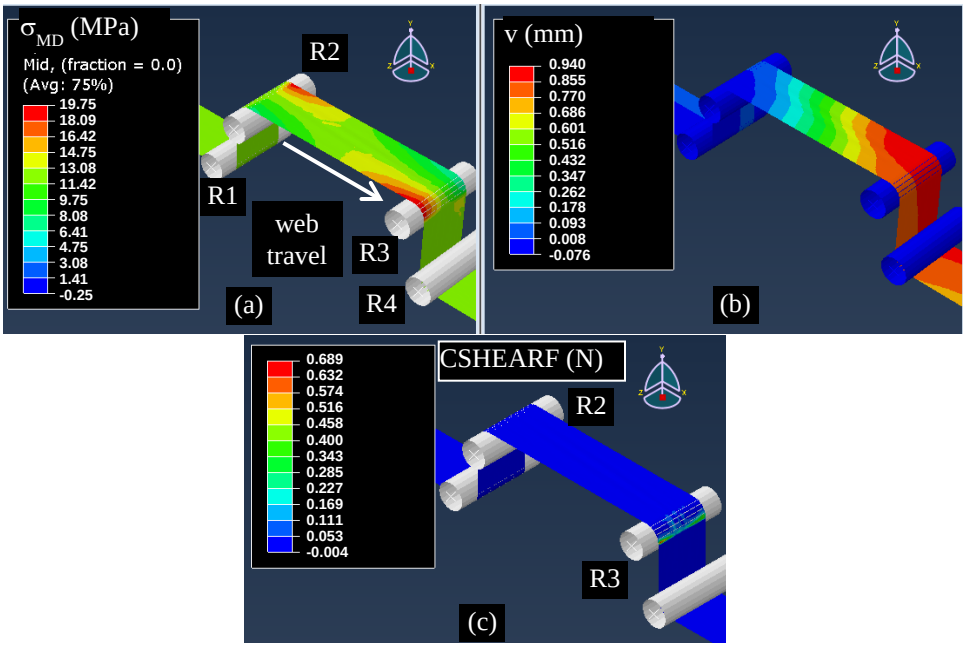

Figure 7 – Dynamic simulation of a web approaching a tapered roller (m=0.00066 m/m).

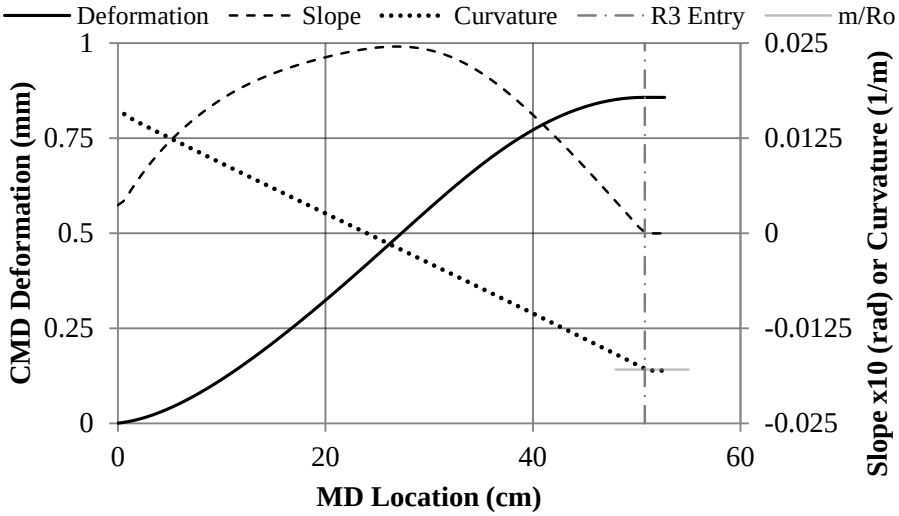

Figure 8 – Deformation, slope and curvature of the elastic axis of the web after steady state conditions were achieved in the simulation shown in Figure 7.

The behaviors of the deformation and the slope of the web on the roller in Figure 8 might appear to be incompatible with the curvature shown. The slope of the elastic axis was obtained by using a central finite difference formula on the lateral deformations. Note that the web enters R3 with zero slope (normal entry) and that the slope remains zero as the web transits the roller without slipping. The curvature of the elastic axis could be calculated by taking the derivative of the slope with respect to the MD and in fact this would be accurate for the web in the free span. This would yield an erroneous result of zero for the curvature of the web in contact with the roller. If the web on the roller had zero curvature it would be the unstressed web whose lateral deformation was a function of wrap angle shown in Figure 5(b). For the web to track directly over the roller, as required by steady state stick behavior and shown by the dashed line in Figure 5(b), the constant curvature of -0.01794 m^{-1} had to exist in the web on the roller. The curvature shown in Figure 8 was obtained by first interrogating the section force/moment field output provided by Abaqus[1] at several points on the elastic axis. These bending moments were then divided by the bending stiffness (EI) of the web to produce the curvature shown in Figure 8. The web tension and bending moment in the web on the roller produces MD stresses that vary linearly in the CMD as shown in Figure 7(a) from 6.08 to 19.1 MPa (882 to 2770 psi) over the web width. It is this MD stress variation over the web width that has allowed the web to conform to the linear taper of roller radius over the web width. The web has taken the shape of the conical roller surface which allows it to directly pass over the roller with no CMD slippage, as shown in the dashed web path in Fig 5(b).

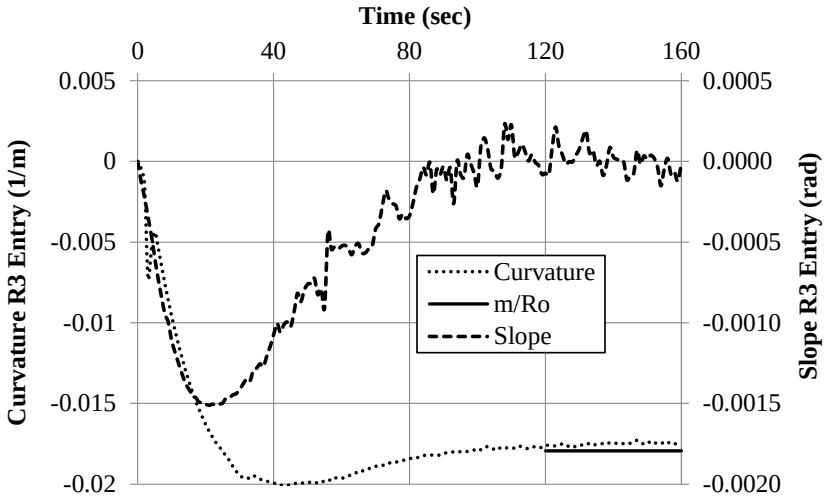

Figure 9 – Rate at which steady state boundary conditions are attained in the simulation shown in Figure 7.

The rate at which boundary conditions {3C} and {8} converge in time is shown in Figure 9. It is apparent the convergence is related to the dynamic time constant of the free span. The span length of 50.8 cm (20 in) divided by the transport velocity of the simulation (1.27 cm/s) produces a time constant of 40 s. Note that convergence of boundary conditions {3C} to 0 radians and {8} to -0.0178 m^{-1} occurred essentially at 3 time constants (120 s).

A Cambered Web Transiting Aligned Cylindrical Rollers

A cambered web is a web whose length varies in the CMD. If this length variation is linear and a length of the web is swept out on a flat surface the web will take the shape of a curved beam of constant radius (ρ_o) in the unstressed state. In Figure 10(a) an unstressed cambered web is shown with long and short sides.

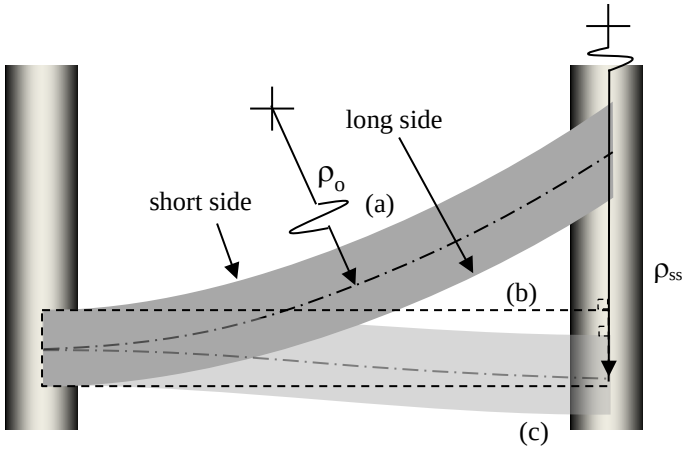

Figure 10 – A Cambered Web: (a) in an undeformed state (b) deformed to a straight path and (c) deformed to steady state path.

The camber radius ρ_o is associated with the undeformed shape of a beam. Curvature is defined as the bending moment at some location in a beam divided by the bending stiffness (EI): $\frac{d^2v}{dx^2} = \frac{M(x)}{EI}$. There is no bending moment applied to the undeformed web and hence there is no curvature. To deform the unstressed web to the straight path would require a constant bending moment (M) of magnitude $-EI/\rho_o$ to be applied to the web (the negative sign is consistent with the convention that a negative moment causes compression on the lower surface of a beam). Hence, the straight web has curvature of magnitude $-M/EI$ or $-1/\rho_o$. It is said the cambered web steers toward the long side. Tests have shown [6,7,8] the cambered web steers laterally beyond the straight web position to a steady state position as shown in Figure 10(c).

The differences in these deformed states are critical when reviewing the state of the literature on cambered web steering. The downstream moment boundary condition (M_L=0) defined by Shelton [1] in Equation {5} is not applicable to the cambered web when steady state lateral deformation has been achieved. It has been assumed that the web span is bounded by two well-aligned cylindrical rollers. For steady state conditions to exist the web must normally enter the downstream roller and thus from boundary condition {3C} θ_j must equal zero. There will be a non-zero steady state moment at the downstream roller associated with deformed state of the cambered web as shown in Figure 10(c). That moment or curvature may be unique from the moment/curvature required to allow the web to track in a cylindrical path around the downstream roller without slipping. Several of the cambered web modeling efforts [9, 10,11, 12] employ Shelton's boundary condition (Equation {5}) and are thus incorrect. Shelton [1] proved this boundary condition was applicable to a straight web entering a misaligned roller but not for a cambered web. Swanson [2] stated the curvature was zero under high friction

conditions and was equal to M_o/EI under low friction conditions based on empirical observation. Per the discussion herein the total curvature is zero only when the web is in the undeformed case of Figure 10(a) and to enforce curvature that would straighten the web (M_o/EI) per Figure 10(b) would require high friction conditions. Swanson did state the downstream curvature was bounded in the range $[0,1/\rho_o]$ which remained valid in his later investigation [8] although the friction levels that produced these curvatures were found to be opposite of the previous investigation. Other investigations concluded that lateral steerage of cambered webs in steady state occurred as a result of higher order effects such as shear, web slackness, and trough instability [9, 12, 13, 14, 16]. Brown [15] developed a beam model to represent a cambered web span. He accounted for the shear strain being non-zero in boundary condition {3B} and for potential misalignment at the downstream roller. He developed an equation for the moment in the web entering the downstream roller which was found to approach EI/ρ_o when examined for the cases herein where the surface velocities of the upstream and downstream rollers were equal.

Swanson [8] reported the results of cambered web steering tests. In these tests cambered webs were cut from a wider web using slitting blades mounted on a stage driven in the CMD by a linear motor. Camber can also be produced as a result of creep of webs in wound rolls with web thickness variation in the CMD. The advantage of Swanson's method was that sections of cambered web with radii ρ_o could be cut for controlled tests as shown in Figure 11(a) with cut sections of straight web in between. These tests employed long web spans where the effects of shear strain on lateral deformations were minimal.

After the camber was cut, the web passed over a position guide into a test span of length L as shown in Figure 11(b). The position guide was used to ensure the lateral position of the web entering the test span could be held constant. The null setting for the edge sensors was established as straight web with no camber was passing through the test section. The chord length of the camber (CL) was established as the camber was cut and was set approximately 4 times the span length (L) of the test section. Webs respond to dynamic disturbances much as a first order dynamic system would react to a step input. Webs typically have very little mass which minimize internal inertial loads and allows the approximation of a first order system. After 4 times the test span length L of either straight web or cambered web passed through the test section the measured lateral deformations (v_1-v_5) should have been at 98.2% of their steady state values. Thus in these tests the steady state deformations of a cambered web were being compared to the steady state deformations of a straight web. This is similar but not identical to a comparison of the steady state deformation shown in Figure 10(c) compared to the straight web in Figure 10(b). As either a section of straight or cambered web would enter the test sections each sensor output (v_i) would begin an exponential change to a steady state value of the form $v_i(1-e^{-t/\tau})$ where t is the elapsed time from the beginning of the event and τ is the dynamic time constant for the web span. As the straight web entered the test section, the measured lateral deformations from the 5 sensors ($v_{1\text{-}5}$) would successively approach zero. As the cambered web would enter the test section the 5 sensors would rise and saturate at unique values of lateral deformation. These values were the relative deformations between the steady state deformations of the cambered and straight webs. These tests were conducted for a polyester web 51 μm (0.002 in) thick and 15.24 cm (6 in) wide. The test span was adjustable but tests began with a span length L of 152.4 cm (60 in). Young's modulus was measured at 4.48 GPa (650 ksi). The web velocity (V) was set low 7.62 mpm (25 fpm) to avoid air entrainment between the polyester and the bare aluminum roller surfaces. The dynamic time constant was $\tau=L/V=12$ s. The rollers were

7.37 cm (2.9 in) in diameter. As the testing begun no steering was witnessed for the cambered web. Steering towards the long side was witnessed when the bare aluminum rollers were covered with high friction tape (Tesa[2] 4863 or 3M[3] 5461). Thus it appeared that high friction force capability between the web and rollers is a requirement to induce measurable steering. The Tesa tape in contact with a polyester web produces a static friction coefficient of 2 and the 3M tape in contact with polyester can produce friction coefficients of 4 or greater per ASTM D1894. It should be noted that Shelton [6] covered his test rollers with 3M[3] Scotch-Tred® in earlier tests on polystyrene cambered web belts which produced high friction and steerage.

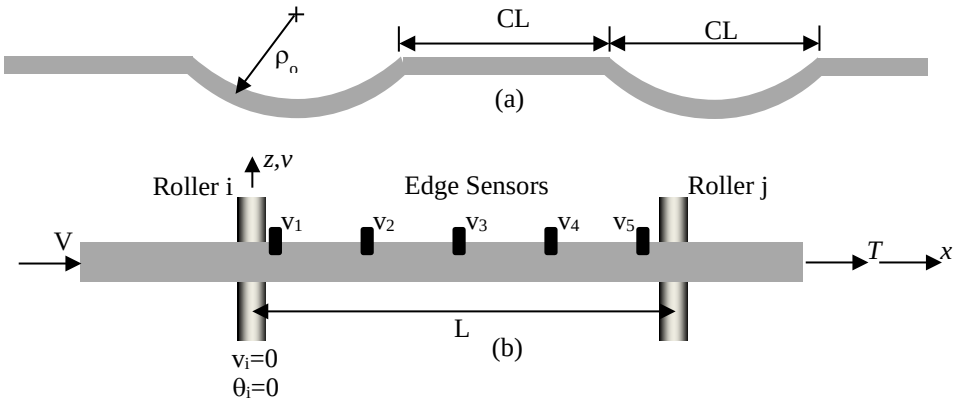

Figure 11 – Swanson Camber tests: (a) camber slit into web (b) test section where steering was measured.

The cambered web approaching an aligned cylindrical roller has both similarity and uniqueness from the problem of a straight web entering a downstream tapered roller. The similarity is that in both cases the web is being steered due to a non-zero curvature in the web as it enters the downstream roller. The uniqueness is the source of the curvature. The straight web approaching a tapered roller had a curvature induced by the downstream roller due entirely to the geometry of the tapered roller (m/R_o) that resulted in the steering per Equation {9}. The camber in the cambered web is the source of a variable web curvature at the downstream roller. This curvature varies with the deformation of the web.

Equation {2} can be used to model the lateral deformation between the steady state (Figure 10(c)) and straight (Figure 10(b)) deformed shapes. It will be assumed that the elastic axis of the web enters the upstream roller at a constant lateral deformation that can arbitrarily be set at zero (v_i=0, {3A}) as a result of the upstream position guide. Furthermore it is assumed that the elastic axis of the web enters the upstream roller normally and due to the high friction condition does not slip appreciably at the exit to the roller (θ_i=0 {3B}). In steady-state normal entry is expected at the downstream roller (θ_j=0 {3C}). The final boundary condition is the change in curvature between the straight and steady-state deformed shapes of the web shown in Figs. 10(b) and (c), respectively:

[2] Tesa Tape Inc., 5825 Carnegie Boulevard, Charlotte, N.C. 28209, USA
[3] 3M Company, 2501 Hudson Rd, Maplewood, MN 55144, USA

$$\left.\frac{d^2v}{dx^2}\right|_{x=L} = \left.\frac{1}{\rho_o} - \frac{1}{\rho_{ss}}\right|_{x=L} = \left.\frac{1}{\rho_\Delta}\right|_{x=L} \quad \{12\}$$

Using boundary conditions {3A} and {3B}, {3C} with θ=0 and {12} the 4 unknowns (A-D) in Equation {4} can now be determined:

$$v(x) = \frac{EI}{\rho_\Delta T}\left[\cosh\left[\frac{\lambda x}{L}\right] - 1 + \coth\left[\frac{\lambda}{2}\right]\left(\frac{\lambda x}{L} - \sinh\left[\frac{\lambda x}{L}\right]\right)\right] \quad \{13\}$$

From Equation {13}, the slope of the web throughout the free span can be determined:

$$\theta(x) = \frac{dv}{dx} = \frac{L}{\rho_\Delta \lambda}\left[\sinh\left[\frac{\lambda x}{L}\right] - \coth\left[\frac{\lambda}{2}\right]\left(\cosh\left[\frac{\lambda x}{L}\right] - 1\right)\right] \quad \{14\}$$

The curvature can be determined throughout the span as well:

$$v''(x) = \frac{d^2v}{dx^2} = \frac{1}{\rho_\Delta}\frac{\sinh\left[\frac{\lambda}{2}\frac{L-2x}{L}\right]}{\sinh\left[\frac{\lambda}{2}\right]} \quad \{15\}$$

Equations {13-15} represent relative changes in lateral deformation, slope and curvature between the straight and steady state deformed shapes of Figs. 10(b and c). If the deformed radius of curvature ρ_Δ was known, the lateral deformation {13}, the slope {14} and the curvature {15} throughout the web span would be known. The total curvature resulting from deforming the web from the undeformed shape Figure 10(a) to the steady state Figure 10(c) can be inferred from Equations {12} and {15}:

$$v''(x)_{total} = \frac{1}{\rho_o} + \frac{1}{\rho_\Delta}\frac{\sinh\left[\frac{\lambda}{2}\frac{L-2x}{L}\right]}{\sinh\left[\frac{\lambda}{2}\right]} \quad \{16\}$$

The deformed radius of curvature ρ_Δ can be deduced from the data of Swanson [8] for the cases tested in which rollers were covered with Tesa 4863 high friction tape. The deformed radius of curvature ρ_Δ was varied in Equation {13} until Swanson's measured deformations at edge sensor v_5 in Figure 11(b) were achieved. The steady state radius of curvature at the entry of the downstream roller ρ_{ss} could be determined using Equation {12}. Also Equation {13} could be used to extrapolate the test deformations to the downstream roller (v_j). These results are presented in Table 1. The average lateral deformations from Swanson's tests and that produced by Equation {13} are shown in Figure 12. Note that in general the test data and the deformations given by Equation {13} agree well and improve at higher web tension. Equation {13} incorporates boundary conditions {3A, 3B, 3C (θ_j=0)} and {12} and produces lateral deformations comparable to the test data from the 5 sensors in the test span. This provides confirmation the boundary conditions are reasonable.

It has been shown that the lateral deformations of a cambered web depend on knowledge of a boundary condition which is the deformed radius of curvature of the web (ρ_Δ) at the downstream roller {13}. This deformed radius of curvature is unknown. For stick conditions to exist between the web and roller at the entry to R2 the radius of curvature of the web must transition to a value equal in magnitude but opposite in sign to the radius of curvature that was initially cut into the web (ρ_o). The curvature in the web will remain constant at that value ($-1/\rho_o$) throughout the arc of contact of the web that is

in stick conditions with the roller. This will allow points in the web to pass directly over the downstream roller with no lateral deformation.

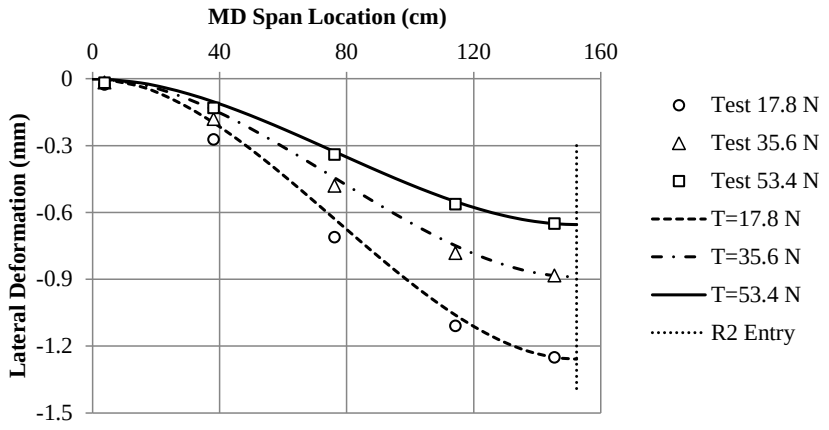

Figure 12 – Swanson camber tests (ρ_o=150 m) with Tesa high friction tape on rollers [8].

T (N)	17.8	35.6	53.4
v_j (mm)	-1.258	-0.889	-0.655
ρ_Δ (m)	-305	-427	-574
ρ_{ss} (m)	-296	-231	-203

Table 1 – Radii of curvatures and lateral deformations at the downstream roller inferred from Swanson's test deformations [8].

Dynamic simulations were first conducted by Fu [20] of the Swanson camber test cases. Fu simulated a web position guide (that existed in the tests) to steer the cambered web shown in Figure 11(a) to a fixed lateral position prior to entering the test section. The web was then allowed to steer laterally in the test section where the lateral deformations resulting from web camber could be studied. Fu's explicit simulation of a web position guide was unique in the literature. While the simulations yielded results comparable to the test data further accuracy was sought to better define the boundary conditions. Improved simulations were conducted using the standard dynamic implicit solver in Abaqus[1]. The simulation begins with the web achieving the constant MD stress level and velocity shown in Figure 13. The web thermal MD expansion coefficient (α) was set at $1.7*10^{-5}$ m/m/ºC. The CMD expansion coefficient was set at zero. A linear temperature variation across the web width was introduced to induce a web camber. The change in temperature required to induce the desired camber of 150 m was $\Delta T=W/(\alpha*\rho_o)= 0.1524/(1.7*10^{-5}*150)=59.8$ ºC. The temperature variation began half way through the wrap of the web about roller R1, continued through the test section and then was removed half way through the wrap of the web about roller R2. The "long" edge of the cambered web had the highest temperature of 29.9 ºC. This temperature variation across the web width varied from zero to the variation shown in Figure 13 in the first second of the simulation after the web velocity and tension had been achieved. The

thermally induced camber in the test section eliminated the need to simulate the web guide and provided the accuracy in results desired.

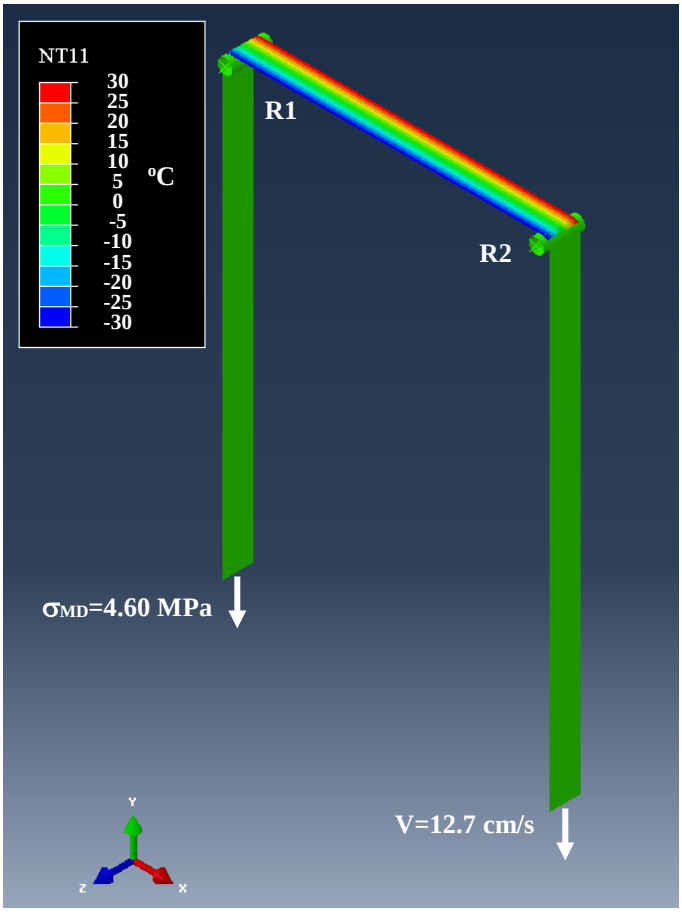

Figure 13 – Dynamic Simulation of Cambered Web Steering.

Steady state results from the end of the simulation are shown in Figure 14 for the case where the web tension was 35.6 N. The MD stresses shown in Figure 14(a) show a decreasing bending moment in the web from roller R1 to R2. The lateral deformations in Figure 14(b) show the web leaving roller R1 with zero lateral deformation and increasing until entry of R2, note that steering towards the longer edge occurred as demonstrated in tests. The web is shown to be in nearly full stick behavior on R1 and R2 with small regions of slip at the exit of R1 and the entry of R2 in Figure 14(c).

In Figure 15 the deformation, slope and curvature of the elastic axis of the web at steady state are shown for the simulation results of Figure 14. The simulation shows the lateral deformation at the exit of roller R1 is zero and thus boundary condition {3A} is satisfied. At the entry to roller R2 the simulation shows the lateral deformation of the web is -.783 mm whereas the average test results extrapolated to the entry of R2 was -.889 mm (11.9% error). While the error is considerable, the shape of the lateral deformation is consistent with the test data captured by the 5 sensors in the test span shown in Figure 12.

The simulation shows the slope of the elastic axis is slightly non-zero ($5.76*10^{-5}$ rad) as the web exits roller R1. Thus boundary condition {3B (θ_i=0)} may be reasonable but not exact in this case. The elastic axis appears to enter roller R2 normally and thus boundary condition {3C} is satisfied as would be required for steady state behavior to be obtained. Perhaps most interesting is the curvature in Figure 15 where step changes in curvature occur at the exit of roller R1 and the entry to roller R2. These abrupt changes in curvature are due to MD contact shear forces between the web and roller at the exit of R1 and the entry of R2. On the rollers R1 and R2 the curvature is what would be required to deform the unstressed cambered web to a deformed straight web that can pass directly over the cylindrical rollers without slip (-1/150 m = $-6.66*10^{-3}$ m^{-1}). At the entry to R2 the curvature is $-4.61*10^{-3}$ m^{-1}, thus the steady state radius of curvature -217 m, which is within 6.1% of the steady state radius of curvature inferred from test data in Table 1. The deformed curvature needed for Equation {13} would be:

$$\left.\frac{1}{\rho_\Delta}\right|_{x=L} = \frac{1}{\rho_o} - \left.\frac{1}{\rho_{ss}}\right|_{x=L} = \frac{-1}{150} - \left.\frac{-1}{218}\right|_{x=L} = -2.06 * 10^{-3} m^{-1} \quad \rho_\Delta|_{x=L} = -486m \quad \{17\}$$

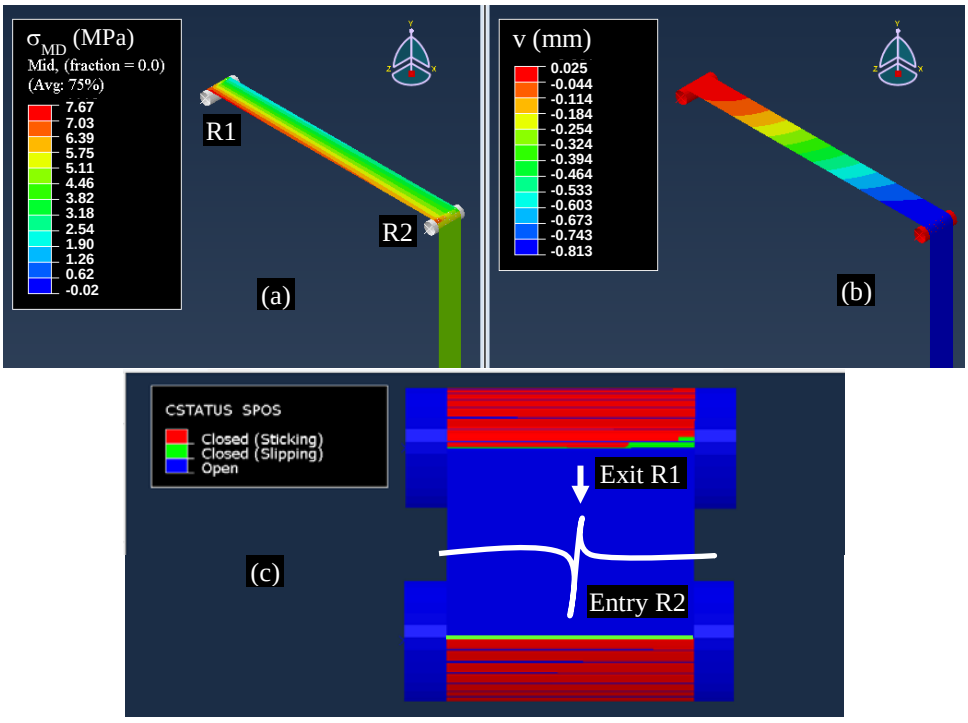

Figure 14 – Simulation Results at Steady State (T=35.6 N).

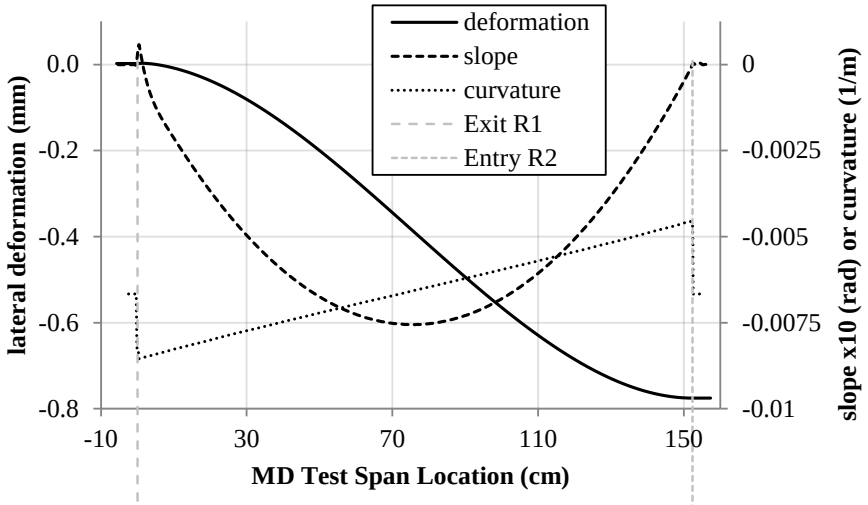

Figure 15 – Deformation, slope and curvature of elastic axis at steady state (T=35.6 N).

If this curvature is input to Equation {13} in conjunction with boundary conditions {3A-3C} the lateral deformation of the web at the entry to R2 can be predicted as -0.781 mm which compares nicely with the -0.783 mm result from the simulation. Thus the results of the simulation with those of Equation {13} agree nicely with the caveat that the simulation was required to produce the curvature boundary condition as the web entered roller R2 {16}.

The simulations also provide explanation with regard to why the lateral steering occurs. In the derivation of the curvature boundary condition {12} for the cambered web, the intermediate straight web shape in Figure 10(b) was used. Note the straight web enters the downstream roller normally and if the straight deformed state physically occurred there would be no lateral deformation toward the long edge due to camber. The slope and lateral deformation at several instants in time from the simulation are shown in Figure 16. The elastic axis of the web is straight at zero seconds, but the web velocity and MD stress shown in Figure 13 had already been achieved at this time. The temperature variation was increased linearly from zero to the variation shown in Figure 13 one second later. From that time forward the web never deformed into the straight web shown in Figure 10(b). Thus the straight deformed web shown in Figure 10(b) is never a physical reality in the simulation after the camber is induced. Note the slope and the lateral deformation are exponentially reaching their steady state values through time $(1-e^{-t/(L/V)})$.

A comparison of the lateral deformations from Swanson's tests [8], the Abaqus simulations and Equation {13} are shown in Figure 17. The deformations from Equation {13} required the deformed radii of curvatures (ρ_Δ) that were determined from the Abaqus simulations and are shown in Table 2. The simulations invoke no assumptions of boundary conditions whereas Equation {13} employs boundary conditions {3A}, {3B}, {3C} $\theta_j=0$, and ρ_Δ {12} from Abaqus in Table 2. Note that Abaqus and Equation {13} produce very similar results throughout the web span with the agreement improving at higher web tensions.

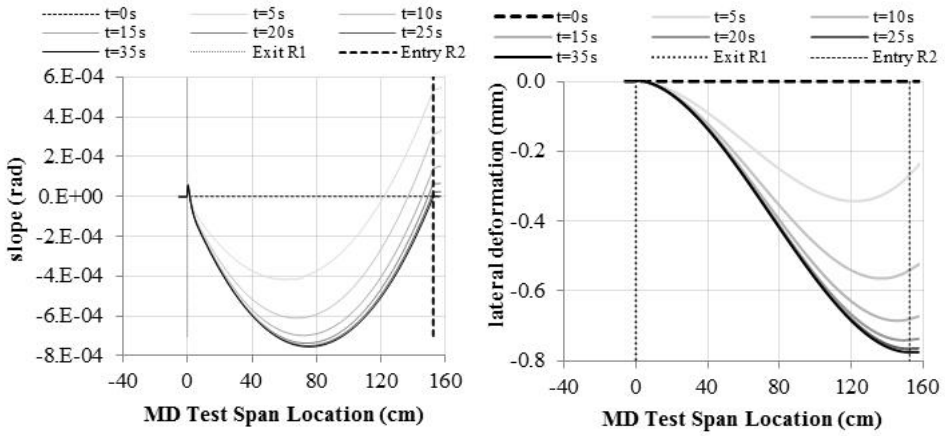

Figure 16 – Deformation and slope of elastic axis through time (T=35.6 N).

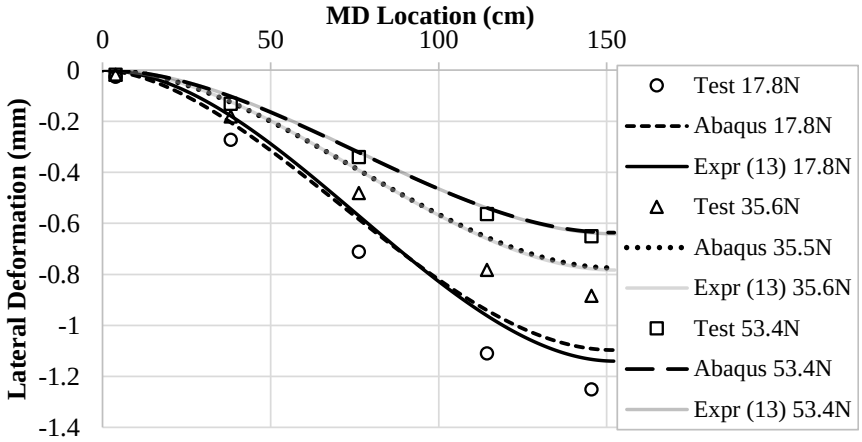

Figure 17 – Lateral deformations from Abaqus simulations, Equation {13} and test data.

T (N)	17.8	35.6	53.4
v_j (mm)	-1.14 (9.4%)	-.783 (11.9%)	-0.641 (2.1%)
ρ_Δ (m)	-336 (10.2%)	-485 (13.6%)	-586 (2.1%)
ρ_{ss} (m)	-271 (8.4%)	-217 (6.1%)	-202 (0.5%)

Table 2 – Radii of curvatures and lateral deformations at the downstream roller inferred from Abaqus simulation results and Equation {13}.

The total curvature and slope of the web entering the downstream roller R2 are shown in Figure 18. Note the web has obtained normal entry with roller R2 within 36 s which is 3 time constants of the free span. The curvature is reaching a steady state value

much earlier. It is surmised that the curvature boundary condition of the web at entry to R2 involves the time constant of the web transiting the roller which is 0.46 s.

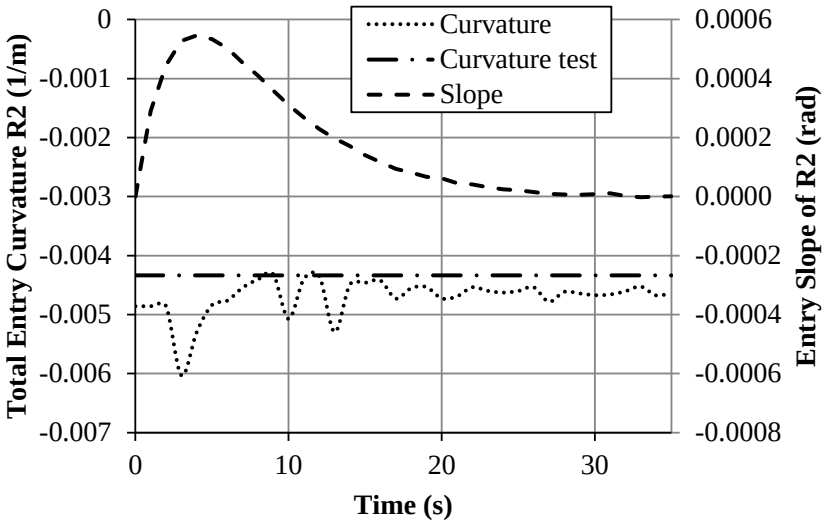

Figure 18 – Rate at which steady state boundary conditions are attained in the simulation shown in Figure 12.

CONCLUSIONS

It has been demonstrated that Equation {2} can be used to model the steady state lateral deformations of a web in a free span for the cases where the downstream roller is misaligned {4} or tapered {9}. The boundary conditions for the span entering the misaligned roller included {3A}, {3B}, {3C} and a zero curvature boundary condition {3D} at the downstream roller required for steady state conditions (i.e. no CMD velocity). The free span bounded by aligned rollers where the downstream roller was tapered linearly in radius with respect to the CMD had similar boundary conditions {3A}, {3B} and {3C (θ_j=0)}. A constant curvature boundary condition {8} was defined to constrain the web to track directly over the downstream roller with no slippage or CMD velocity to attain steady state lateral behavior. In these two cases the rollers that bounded the web span and the assumption of no slip dictated the boundary conditions that produced the steady state lateral deformation of the web. The case of a cambered web has similarity to these cases in the first three boundary conditions {3A}, {3B} and {3C (θ_j=0)}. The cambered web also has a curvature boundary at the entry to the downstream roller {12} but differs from the other cases in that this curvature is dependent on the deformed state of the cambered web. Web tension, web material properties, initial camber and friction forces at the web entry to the downstream roller all will affect the deformed curvature which allows the web to reach steady state conditions. MD slippage is required at the web entry to the downstream roller such that the curvature can instantaneously change from the level which brought the lateral deformation to steady state ($1/\rho_\Delta$) to a level that allows the deformed cambered web to track directly over the roller with no lateral velocity ($1/\rho_0$). To determine the deformed radius of curvature at the downstream roller (ρ_Δ) requires a method that can establish the equilibrium of the internal

forces in the deformed web and the external forces due to slip as the web enters the downstream roll and the stick behavior of the web on the roller. Only laboratory tests [8] and dynamic simulations (Abaqus) have shown that capability.

ACKNOWLEDGEMENTS

The authors would like to acknowledge the industrial sponsors of the Web Handling Research Center for their support of the research reported herein. They would also like to acknowledge those who have contributed to the research to determine why cambered webs steer laterally in R2R process machines. They would like to individually acknowledge J. J. Shelton (deceased) of Oklahoma State University and R. P. Swanson of 3M Company. These individuals provided proof that cambered webs steer in process machines in the laboratory. This proof provided encouragement for many to study why the cambered web steers. Finally the authors would like to dedicate this paper to the memory of John J. Shelton. Dr. Shelton carried the torch for cambered web research for many years.

REFERENCES

1. Shelton, J. J., and Reid, K. N., "Lateral Dynamics of a Real Moving Web," ASME J. Dyn. Syst., Meas., Control, Vol. 93, No. 3, 1971, pp. 180-186.
2. Shelton, J. J., and Reid, K. N., "Lateral Dynamics of an Idealized Moving Web," ASME J. Dyn. Syst., Meas., Control, Vol. 93, No. 3, 1971, pp. 187-192.
3. Good, J. K., "Shear in Multispan Web Systems," Proceedings of the Fourth International Conference on Web Handling, Web Handling Research Center, Stillwater, Oklahoma, June 1-4, 1997, pp. 264-286.
4. Shelton, J. J., "Interaction between Two Web Spans Because of a Misaligned Downstream Roller," Proceedings of the Eighth International Conference on Web Handling, Web Handling Research Center, Stillwater, Oklahoma, June 5-8, 2005, pp. 101-122.
5. Yurtcu, H. H., Beisel, J. A., and Good, J.K., "The Effect of Roller Taper on Webs," TAPPI Journal, Vol. 11, No. 11, November 2012, pp. 31-38.
6. Shelton, J. J., "Effects of Web Camber on Handling," Proceedings of the Fourth International Conference on Web Handling, Web Handling Research Center, Stillwater, Oklahoma, June 1-4, 1997, pp. 248-263.
7. Swanson, R. P., "Mechanics of Non-Uniform Webs," Proceedings of the Fifth International Conference on Web Handling, Web Handling Research Center, Stillwater, Oklahoma, June 6-9, 1999, pp. 443-459.
8. Swanson, R. P., "Lateral Dynamics of Non-Uniform Webs," Proceedings of the Tenth International Conference on Web Handling, Web Handling Research Center, Stillwater, Oklahoma, June 7-10, 2009, pp. 531-554.
9. Benson, R. C., "The Influence of Web Warpage on Lateral Dynamics of Webs," Proceedings of the Fifth International Conference on Web Handling, 1999, pp. 461-472.
10. Olsen, J. E., "Lateral Mechanics of an Imperfect Web," Proceedings of the 6th International Conference on Web Handling, ed. Good, J. K., 2001, pp. 457-468.
11. Olsen, J. E., "Lateral Mechanics of an Imperfect Web," Journal of Pulp and Paper Science, 2002, pp. 310-314.

12. Benson, R. C., “Lateral Dynamics of a Moving Web with Geometrical Imperfection,” Journal of Dynamic Systems, Measurement, and Control, Vol. 124, March 2002, pp. 25-34.
13. Olsen, J. E., “Shear Effects and Lateral Dynamics of Imperfect Webs,” Proceedings of the 7th International Conference on Web Handling, ed. Good, J. K., 2003.
14. Olsen, J. E., “Lateral Mechanics of Baggy Webs at Low Tensions,” Proceedings of the 8th International Conference on Web Handling, ed. Good, J. K., 2005, pp. 25-37.
15. Brown, J. L., “Effects of Concave Rollers, Curved-Axis Rollers and Web Camber on the Deformation and Translation of a Moving Web,” Proceedings of the 8th International Conference on Web Handling, ed. Good, J. K., 2005, pp. 61-80.
16. Jones, D. P., “Web Sag and the Effects of Camber on Steering,” Proceedings of the 9th International Conference on Web Handling, ed. Good, J. K., 2007, pp. 353-370.
17. Rivello, R. M., Theory and Analysis of Flight Structures, 1st ed, McGraw Hill, 1969, pp. 158-159.
18. Lorig, E. T., AISE (Association of Iron and Steel Engineers) Annual Convention, Cleveland, Ohio, 1950.
19. Webb, D. K., “Prediction of Web Wrinkles Due to Misalignment of a Downstream Roll in a Web Span,” M.S. Thesis, Oklahoma State University, Dec. 2004, pp. 19-20.
20. Fu, B., and Good, J. K., “Explicit Simulations of Cambered Web Steering,” Proceedings of the Thirteenth International Conference on Web Handling, Web Handling Research Center, Stillwater, Oklahoma, June 7-10, 2015.